RSC Advances

ROYAL SOCIETY OF CHEMISTRY

www.rsc.org/advances

Table of contents entry:

Novel superior antibiotics, amine *N*-halamine microspheres based on 2,2,6,6-tetramethyl-4-piperidinol, were synthesized via the radical copolymerization, and their bactericidal effects were systematically studied.

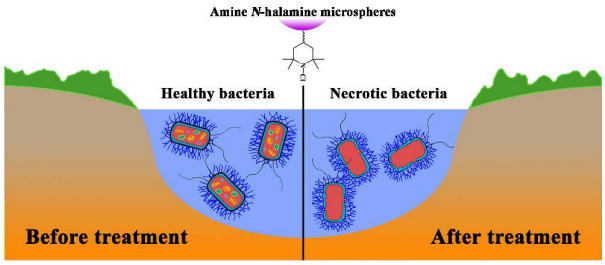

Journal Name

RSCPublishing

ARTICLE

Design, synthesis and biocidal effect of novel amine *N*-halamine microspheres based on 2,2,6,6-tetramethyl-4-piperidinol as promising antibacterial agents

Cite this: DOI: 10.1039/x0xx00000x

Received 00th January 2012,
Accepted 00th January 2012

DOI: 10.1039/x0xx00000x

www.rsc.org/

Chenghao Li,[a] Linyan Xue,[a] Qian Cai,[a] Sarina Bao,[a] Tianyi Zhao,[b] Linghan Xiao,[c] Ge Gao,[b] Chokto Harnoode[a] and Alideertu Dong*[a]

Novel superior antibiotics, amine type *N*-halamine microspheres based on 2,2,6,6-tetramethyl-4-piperidinol, were firstly synthesized by the aid of the radical copolymerization for deactivating pathogenic bacteria. Effect of copolymerization period on particle size and copolymer component of the products were well elucidated. The oxidative chlorine content in amine *N*-halamine microspheres was determined by the modified iodometric/thiosulfate technique. Effect of chlorination period on oxidative chlorine content was investigated as well. Bactericidal behaviour of the products on bacterial strain was tested by selecting *Staphylococcus aureus* (*S. aureus*) and *Escherichia coli* (*E. coli*) as model pathogenic bacteria. Antibacterial assessment including the plate counting technique, zone of inhibition study, and antibacterial kinetic test demonstrated that amine *N*-halamine microspheres exerted powerful bactericidal capability. Effects of the contacting period, particle size, and oxidative chlorine content on antimicrobial activity were also established. High stability of amine *N*-halamine microspheres as a function of soaking period was confirmed finally. Such a systematic investigation of amine type *N*-halamines provides us a novel idea of making them the promising candidates for deactivating bacteria or even disease control.

1. Introduction

Undoubtedly pathogenic bacteria are responsible for most of the world lethal diseases.[1] Developing effective antibiotics with a wide spectrum of biocidal activities is hence urgently necessary. *N*-Halamines with nitrogen-halogen covalent bond known for instant and total sterilization towards wide range of microorganisms have recently been of tremendous interest in antimicrobial field.[2-4] Especially, polymer-based *N*-halamines acted as ideal candidates are utilized widely for bactericidal modification of various materials' surfaces such as cotton, nylon, silica gel, and paint etc.[5-8] The popularization of *N*-halamine polymers derives from their inherent advantages such as good stability for long-term use, storage over a wide temperature range, ability to be regenerated in a chlorine solution repeatedly, lack of corrosion, low toxicities, and relatively low expense.[9] As a result, *N*-halamine polymers have proved to be promising in the development of effective antibacterial materials.

N-Halamine polymers can be composed of one or more imide/amide/amine *N*-halamine bond.[10] Despite of efficient biocidal capability, there remain some limitations to *N*-halamines due to their stability.[11] It was reported that the dissociation constant of *N*-halamines in aqueous solution is directly related to their structures in an order of amine < amide < imide, as shown in Table S1. Amine *N*-halamine is the most stable among them. To date, amide and imide *N*-halamines have been extensively reported, but few reports about amine *N*-halamine has been founded. To the best of our knowledge, 2,2,6,6-tetramethyl-4-piperidinol (TMP) famous for photostability has a structurally hindered amine in structure.[12,13] By halogenating, TMP can be readily transformed into amine *N*-halamine for biocidal applications, which caught our attention.

It is accepted that antibacterial capability of *N*-halamines is strongly dependent on their sizes.[14] Nanosize *N*-halamines can show more advantageous biocidal activity than their bulk counterparts due to their smaller size and larger activated surface area.[15] Thus fabricating *N*-halamines with nanosize is an effective way for enhancing antimicrobial capability. Introducing a colloidal template for reducing material size is deemed to be the most effective and controllable technique, especially for studies in which monodispersion is required.[16] Silica, iron oxide, carbon, and polymer microspheres are the popular option as templates to enlarge the activated surface.[17-20] Our group previously developed several imide and amide *N*-halamine microspheres using the colloidal template method.[21-27] Those amide and imide *N*-halamine microspheres possessed excellent biocidal property against the model bacteria such

as *E. coli*, *P. aeruginosa*, *B. subtilis*, and *S. aureus*. For in-depth study, amine *N*-halamine microspheres were also designed and investigated systematically by our group. Synthesizing amine *N*-halamine homopolymer microspheres via the radical homopolymerization of 4-(allyloxy)-2,2,6,6-tetramethylpiperidine (ATMP) was carried out in the beginning. Unfortunately, satisfactory higher molecular weight products can hardly be attained due to the radical "auto-inhibition" effect of allyl structure of ATMP.[28] As a result, copolymerization approach was then taken into account for solving the problem. Methyl methacrylate (MMA) favorable to radical polymerization was selected herein for copolymerizing with ATMP because ester group of MMA can stabilize the radicals and promote the reactivity of allyl monomers towards chain propagation reaction.[29] In this way, MMA not only act as comonomer but also provide poly(methyl methacrylate) (PMMA) template for amine *N*-halamine functionalized microspheres without using any additive colloidal template.

Herein, we developed novel amine *N*-halamine microspheres as potent biocides form 2,2,6,6-tetramethyl-4-piperidinol (TMP) through the modification of PMMA microspheres with *N*-halamine, as shown in Scheme 1. ATMP was firstly synthesized by one-step reaction between TMP and allyl bromide (1) and copolymerized with MMA using radical copolymerization (2) followed by chlorination (3) to obtain amine *N*-halamine microspheres. The as-synthesized novel amine *N*-halamine microspheres have powerful bactericidal activity against both Gram-positive and Gram-negative bacteria. Thanks to the overwhelming bactericidal capability, amine *N*-halamine microspheres can be the ideal candidate for wide significant applications ranged across medical system, water purification, food industry, apparel product, and household sanitation, etc. The immobilization of amine *N*-halamine microspheres by means of physical approach or chemical bonding on materials surface can protect them from the contamination by microorganisms such as pathogenic bacteria, odor-generating bacteria, molds, fungi, and virus, etc. Therefore, this study would be valuable of designing novel biocides and extending the industrial application of amine *N*-halamines.

2. Experimental section

2.1 Materials

2,2,6,6-Tetramethyl-4-piperidinol (TMP) was obtained from Nangong Shenghua Chemicals Co., Ltd. Tetrahydrofuran (THF), ethanol, and petroleum ether were purchased from Beijing Chemical Company. Methyl methacrylate (MMA), anhydrous magnesium sulfate ($MgSO_4$), and potassium persulfate (KPS) were available from Tianjin Chemical Reagent Plant and Shanghai Chemical Reagent Plant, respectively. Sodium hydride (NaH) was obtained from Beijing Hengye Zhongyuan Chemical Co., Ltd. Allyl bromide and sodium hypochlorite (NaClO) were provided from Sinopharm Chemical Reagent Co., Ltd.

2.2 Characterization

^{1}H NMR spectra were recorded on a Bruker AVANCEⅢ-500 NMR spectrometer in DMSO solution, and the chemical shift values were given in parts per million (ppm). FTIR spectra were captured by using a Thermo Nicolet (Woburn, MA) Avatar 370 FTIR spectrometer using KBr pellet method in the range of 400-4000 cm^{-1} to analyze the sample compositions. The transmittance mode at a resolution of 4 cm^{-1} by averaging 32 scans was utilized. The morphology, particle size, surface state, size distribution, and elemental mapping of the samples were observed on a Shimadzu SSX-550 field emission scanning electron microscope (SEM) at 15.0 kV and a Hitachi H8100 transmission electron microscope (TEM) at 200 kV. The samples were dispersed in ethanol with assistance of sonication and casted onto the silicon wafer for SEM and copper grid for TEM characterization, and then were dried at room temperature before examination. X-ray photoelectron spectra (XPS) was carried out on a PHI-5000CESCA system with Mg K radiation.

2.3 Preparation of 4-(allyloxy)-2,2,6,6-tetramethylpiperidine

3.97 g (0.025 mol) of 2,2,6,6-tetramethyl-4-piperidinol (TMP) was mixed with 50 mL of freshly distilled anhydrous THF. The mixture was stirred in a sealed flask under a nitrogen atmosphere at ambient temperature, and then poured into a flask containing 0.66 g (0.0375 mol) of NaH. The reactants were stirred for 30 min, and then 2.40 mL (0.027 mol) of allyl bromide were added dropwise in the mixture. The reactants were stirred for 30 min at ambient temperature and then for 12 h at 65 ^oC under a nitrogen atmosphere. The sodium bromide byproduct was removed by filtration and the THF solvent by distillation. The crude product was added in 50 mL of ultrapure water, and the mixture was extracted with 50 mL of petroleum ether. The organic phase was dried over anhydrous $MgSO_4$, and the solvent was removed by distillation to give the pure ATMP as yellow oil.[30]

2.4 Preparation of poly(ATMP-*co*-MMA) microspheres

0.1 g of potassium persulfate and 150 mL of ultrapure water were added in a 250 mL three-necked flask with a condenser and a N_2 gas inlet, and a mixture of 0.1 g of ATMP dissolved in 3 mL of MMA was added. The reaction mixture was maintained at 75 ^oC with vigorous stirring to obtain poly(ATMP-*co*-MMA) microspheres. Copolymer microspheres with different particle size and component were prepared under the different reaction time.

2.5 Preparation of amine *N*-halamine microspheres

Poly(ATMP-*co*-MMA) microspheres were immersed in a 10 % commercial aqueous sodium hypochlorite solution buffered at pH 7 at room temperature. The as-prepared amine *N*-halamine microspheres were washed thoroughly with a mixture of water and ethanol, and then dried at 40 ^oC for 6 h to remove any remaining free chlorine from the surface of the sample. The oxidative chlorine content of the amine *N*-halamine microspheres was well controlled with different chlorination periods.

2.6 Determination of oxidative chlorine content

Oxidative chlorine content of the amine *N*-halamine microspheres was determined by the modified iodometric/thiosulfate titration

procedure.[31] The percentage of active chlorine (Cl^+ %) for the sample was calculated according to the following equation.

$$Cl^+\% = \frac{35.5}{2} \times \frac{(V_{Cl^+} - V_0) \times 10^{-3} \times 0.01}{W_{Cl^+}} \times 100$$

where V_{Cl+} and V_0 are the volumes (mL) of sodium thiosulfate solutions consumed in the titration of the chlorinated and unchlorinated samples, respectively, and W_{Cl+} is the weight of the chlorinated sample (g).

2.7 Bacterial cultures and growth conditions

In this experiments, *Staphylococcus aureus* (*S. aureus*, ATCC 25923, Gram-positive) and *Escherichia coli* (*E. coli*, ATCC 25922, Gram-negative) were used as model microorganisms to test the antibacterial activities of the samples. Bacteria were grown overnight at 37 ^oC under agitation (250 rpm) in Luria Bertani growth medium. Cells were harvested by centrifugation, washed twice with phosphate-buffered saline (PBS, NaCl, 8.0 g/L; KCl, 0.20 g/L; $Na_2HPO_4 \cdot 12H_2O$, 3.49 g/L; KH_2PO_4, 0.2 g/L; pH 7.4), and diluted to concentrations of 10^{6-7} colony-forming units/mL.

2.8 Antibacterial assessment

70 mg of each sample was dispersed in 0.45 mL sterilized distilled water, vortexed, and then sonicated for 30 min. For antibacterial test, 50 μL of bacteria suspension was added into 450 μL sample suspension, mixed well, and incubated under constant shaking. After a certain period of contact time, 4.5 mL of 0.03 wt % sodium thiosulfate aqueous solution, sterilized by passing through 0.22 μm membrane and exhibited no effect on the growth of bacteria, was added into the reaction suspension to neutralize the active chlorine and stop the antibacterial action of sample. The resulting mixture was mixed well, serially diluted, and then 100 μL of each dilution was dispersed onto LB agar plates. Colonies on the plates were counted after incubation at 37 ^oC for 24 h. Bacteria diluted by di-water in the same way of sample testing (blank solution) worked as negative control.

The inhibition zone study of the product was carried out by a modified Kirby-Bauer technique.[32] The surface of Luria Bertani agar plate and tryptic soy agar plate was overlaid with 1 mL of 10^{8-9} CFU/mL of *E. coli* (ATCC 8099) and *S. aureus* (ATCC 25923). The plates were then allowed to stand at 37 ^oC for 4 h. Amine *N*-halamine microspheres was placed onto the surface of the bacteria-containing agar plate, and gently pressed with a sterile forceps to ensure full contact between the sample and the agar. After incubation at 37 ^oC for 24 h, the inhibition zone around the sample was determined.

3. Results and discussion

3.1 Synthesis and characterization of amine *N*-halamine microspheres

Amine *N*-halamine microspheres as novel superior antibiotics were synthesized facilely by the radical copolymerization of MMA with allyl-functionalized 2,2,6,6-tetramethyl-4-piperidinol followed by chlorination. Scheme 1 represents the synthetic procedure of the amine *N*-halamine microspheres. The target products are available in three steps, and each step is well controlled. Firstly, ATMP was synthesized via the substitution reaction between TMP and allyl bromide (1). The existence of allyl group makes ATMP polymerizable in the presence of initiator KPS. However, a large number of attempts for synthesizing ATMP homopolymer with higher molecular weight via the radical polymerization ended in failure. In response to such a difficulty, MMA was introduced to copolymerize with ATMP because MMA with ester group in structure can stabilize the radicals during the polymerization process. This can promote polymerization proceeding towards chain propagation (2). Finally, amine group of poly(ATMP-*co*-MMA) microspheres transformed into N-Cl covalent bond through the chlorination treatment to form the target amine *N*-halamine polymeric microspheres (3). The oxidative chlorine can provide antimicrobial active site for killing pathogenic bacteria, making amine *N*-halamine microspheres as bactericide candidate for inactivating microorganism in wastewater and even extending to disease control.

^1H NMR of TMP, ATMP, MMA, poly(ATMP-*co*-MMA), and amine *N*-halamine microspheres are shown in Fig. 1. The characteristic fitting signal for solvent DMSO is found at δ = 2.5 ppm.[33] The assignments of the signals in TMP are δ = 1.0, 1.7, 3.8, and 4.4 ppm corresponding to $-CH_3$, $-CH_2-$, >CH-, -OH group, respectively in Fig. 1A.[34] The additional characteristic signals for $-CH_2-$, -CH=, and $=CH_2$ of allyl group are detected at δ = 4.0, 5.9, and 5.2 in Fig. 1B, suggesting the formation of ATMP. Mass spectrogram in Fig. S1 further confirms the successful formation of ATMP. As for MMA (Fig. 1C), the $CH_2=$ group shows signals at δ = 5.8 ppm and 6.0 ppm, and the $-CH_3$ and $O-CH_3$ display the resonance peak at δ = 3.8 ppm and 1.8 ppm, respectively. After copolymerization, the characteristic CH-, CH_2-, and CH_3- signal are observed for poly(ATMP-*co*-MMA) in Fig. 1D, while the $CH_2=C$ signals of ATMP and MMA component can no longer be detected, which reflects the successful formation of poly(ATMP-*co*-MMA) via the radical copolymerization of ATMP with MMA. After chlorination in Fig. 1E, a slight shift is found in $-CH_2-$ and $-CH_3$, which is attributed to the replacement of the N-H bond with N-Cl bond possibly because the latter has a stronger electron-withdrawing effect than the former. These characteristic signals are the effective evidences for the success of amine *N*-halamine microspheres.

Formation of the products was further confirmed by recognizing the characteristic groups using FTIR spectra. As shown in Fig. 2A, TMP shows C-H, O-H, N-H, C-N characteristic peak at around 2929, 2978, 3255, 3158, 3433, and 1232 cm^{-1}, respectively.[34] The spectrum of ATMP in Fig. 2B differs markedly from that of TMP. The new peaks at 1647 and 3080 cm^{-1} for C=C and =C-H stretching vibration are clearly observed.[35] The multiplet of C-O-C stretching is detected within the range of 1070-1170 cm^{-1} corresponding to the newly generated ether bond.[36] These new peaks (C=C, =C-H, and C-O-C) well confirm the fabrication of ATMP from TMP. Fig. 2C exhibits a strong band at 1736 cm^{-1}, which is ascribed to C=O of ester in MMA molecular.[37] The C=C and =C-H stretching vibration at 1622 and 3124 cm^{-1} are also seen in Fig. 2C. After

copolymerization, C-O-C, N-H, N-C, and C=O band corresponding to ATMP and MMA contents still appear, but the C=C and =C-H stretching vibration disappear in Fig. 2D. From the disappearance of the C=C and =C-H characteristic peak, the copolymerization of ATMP with MMA is confirmed. Chlorinated product in Fig. 2E shows almost coincident characteristic spectrum with poly(ATMP-*co*-MMA) microspheres except for the N-H and C-N peak. Almost invisible N-H stretching vibration at about 3435 cm^{-1} is associated with the N-H→N-Cl transformation. This negligible weak N-H peak is likely corresponding to the un-chlorinated amine group inside the microspheres. The characteristic C-N peak shifts slightly from 1242 cm^{-1} in poly(ATMP-*co*-MMA) microspheres to 1244 cm^{-1} in the amine *N*-halamine microspheres spectrum because of the substitution of C-N-H for C-N-Cl.[38] All these are in good agreement with the ^{1}H NMR results.

To realize morphology characterization, SEM and TEM technique were applied. Fig. 3A shows the representative SEM and TEM image of poly(ATMP-*co*-MMA) microspheres before and after chlorination. Obviously, poly(ATMP-*co*-MMA) microspheres are uniform, quasi-monodisperse, spherical, smooth and solid, showing flawless surface without any cracks or degradation. The particle sizes are in a narrow range of 150-210 nm with an average size of 181.8 nm. After chlorination, subtle conglutination, bulge, and ovalization are seen. A size distribution from 150 to 220 nm is obtained, and the average diameter shifted to 187.4 nm. Slight changes in morphology and size are possibly due to the transformation of the amine group into *N*-halamine structures. However, no subversive change is found in spherical shape, suggesting that chlorination has no destructive effect on the structural framework of the samples. Besides, elemental mapping technique was performed to confirm the presence of different elements and the elemental distribution in the products (Fig. 3B). Both poly(ATMP-*co*-MMA) microspheres before and after chlorination treatment show the element Si signal noted as yellow dot, which is from the Si substrate used for sample immobilization. The mapping results of the poly(ATMP-*co*-MMA) microspheres show elemental signal of C, O, and N evenly scattered throughout the whole photos. Unlike poly(ATMP-*co*-MMA) microspheres, the amine *N*-halamine microspheres provide additional signal of element Cl observed as cyan dots, which further confirms the N-H→N-Cl transformation. The elemental analysis is a supplement to FTIR and ^{1}H NMR technique for the evidence for formation of the amine *N*-halamine microspheres.

Detailed data about the chemical composition of the products obtained from XPS spectra are shown in Fig. 4. The poly(ATMP-*co*-MMA) microspheres show C 1s, N 1s, and O 1s, and additional Cl 2p peak appears after chlorination treatment. Two elemental signals Si 2s and Si 2p are likely from the glass support used for sample immobilization.[39] For further identification, the deconvolution of C 1s, N 1s, and Cl 2p energy level was also performed. For both poly(ATMP-*co*-MMA) microspheres and amine *N*-halamine microspheres, the C 1s peak is curved into four divided peaks such as C=O, C-O, C-C, C-N bond.[40] The similar C 1s peak of these two products illustrates that the chlorination treatment has no destructive effect on the polymeric carbon framework. The poly(ATMP-*co*-MMA) microspheres reveal two peak component of -N< and -NH- in N 1s signal peak.[41] After chlorination, -NH- peak is completely replaced by -NCl- peak in the N 1s energy level, suggesting the formation of the amine *N*-halamine microspheres. As expected, no Cl 2p signal is detected for spectrum of poly(ATMP-*co*-MMA) microspheres. Comparatively, the emergence of Cl 2p in amine *N*-halamine microspheres provides conclusive evidence for the N-H→N-Cl transformation.[42]

The antibacterial function of *N*-halamines is based on the transfer of positive halogen from N-X (X = Cl or Br) covalent bond to bacterial cells, and such oxidative halogen has a strong tendency to destruction or inhibition of metabolic processes in microorganisms.[43] Therefore, the antimicrobial behavior of *N*-halamines is inevitably related to N-H→N-Cl transformation. Besides physical techniques such as NMR, FTIR, XPS, the formation of the amine *N*-halamine microspheres was herein further validated by a chemical method, iodometric/thiosulfate titration. It is well-known that the iodometric/thiosulfate titration mainly involves two oxidation-reduction reactions as shown in Fig. 5A.[44] Color change appeared during the iodometric/thiosulfate titration is shown in Fig. 5B. Positive chlorine (B-1) can firstly oxidize iodide ions to produce iodine (B-2), which is corresponding to the first reaction (A-1). The as-prepared iodine can impel chromogenic reaction in starch solution showing blue suspension (B-3). The iodine then can be exhausted by the titrated thiosulfate for colour fading (B-4), which can be explained by the second reaction (A-2). The colour changes are the effective evidences for the oxidation-reduction reactions and the proof for the existence of the amine *N*-halamine microspheres. Beside qualitative characterization, the iodometric/thiosulfate titration can also be utilized as quantitative analysis for determining the active chlorine content of *N*-halamines.

3.2 Effect of copolymerization period on particle size and copolymer component

As for *N*-halamine microspheres, antimicrobial efficiency is strongly dependent on their particle size. Controllable synthesis of monodisperse *N*-halamine microspheres with smaller size hence seems to be quite meaningful. Copolymerization period plays an important role in preparing poly(ATMP-*co*-MMA) microspheres with tunable size via the radical polymerization. In this study, copolymerization period was ranged from 1 h to 6 h, while keeping all other parameters fixed. Extending the aging period has no effect on the samples morphology showing similar spherical shape and smooth surface, while the particle size increases proportionally with copolymerization period (Fig. S2). The detailed data about particle size and size distribution as a function of copolymerization period are summarized in Fig. 6A and Fig. S2. As the time extending from 1 h to 6 h, the average diameter is ranged widely from ~50 nm to ~250 nm. Interestingly, particle size rapidly rises firstly and then slows down as the aging time is further increased. This is likely due to the fact that monomers in reaction system are sufficient at lower copolymerization time (interval Ⅰ), and particle growth is sensitive to the aging time. When aging time is further increased, the amount of free monomers decreases and as a result particle growth slows down (interval Ⅱ). It is acceptable that smaller size can provide larger surface area, which could offer more active *N*-halamine site to kill bacteria (Table S2). Therefore, such size-controllable synthesis

of poly(ATMP-*co*-MMA) microspheres provides the possibility of fabricating amine *N*-halamine microspheres with the required sizes.

Effect of copolymerization period on structural ATMP content in poly(ATMP-*co*-MMA) microspheres was estimated quantificationally from FTIR technique by capturing the intensity of N-H bond of ATMP and C=O bond of MMA in copolymer. Fig. 6B shows the plot of $A_{N-H}/A_{C=O}$ *vs.* copolymerization period, where A_{N-H} and $A_{C=O}$ represent the peak area of the 3443 and 1730 cm^{-1} band, respectively. The drastic increase of $A_{N-H}/A_{C=O}$ value with aging time from 0 to 2 h is obtained, reflecting the increase in ATMP content within 2 h of copolymerization period. The most possible reason for such phenomenon is the nature of ATMP and MMA monomer towards the radical polymerization.[45] The allylic structure in ATMP prevents chain propagation reactions due to the autoinhibition effect during radical polymerization.[28] MMA is favourable to radical polymerization because the ester can stabilize the radicals and enhance the reactivity of the monomer towards chain propagation reaction.[29] Therefore, MMA is more active than ATMP towards chain propagation reaction in the initial stage, which results in the lower ATMP content in the beginning. Then the radicals from ATMP can be stabilized and even promoted by MMA with extending aging time to 2 h, resulting in remarkable increase of ATMP content in copolymers. However, gradual decrease is observed in $A_{N-H}/A_{C=O}$ value after 2 h possibly because of the exhaustion of ATMP monomer resulting in the decrease of ATMP content despite of particle growth. Taken particle size and ATMP content into consideration, copolymerization period of 2 h is selected as optimum point in this study for further investigation.

3.3 Effect of chlorination period on oxidative chlorine content

It is widely acknowledged that halogen transfer is the most acceptable biocidal mechanism of *N*-halamines.[46] Therefore, chlorine content plays decisive role in governing the antimicrobial capability of *N*-halamines. The N-H structure can be transformed facilely into N-Cl group upon treatment with sodium hypochlorite to obtain the target *N*-halamine product.[47] Herein effect of chlorination period on active chlorine content in the amine *N*-halamine microspheres was evaluated. Fig. 7 shows the developing trend of the percentage of oxidative chlorine with extending chlorination period ranged from 0 to 16 h. Overall, sharp increasing trend in chlorine loading is detected within the lower chlorination time range, and oxidative chlorine content slows down gradually when further extends chlorination period. In detail, the sample reaches merely 0.53 % chlorine content upon chlorination treating for 15 min, while as high as 1.17 % chlorine content after 2 h. Interestingly, the chlorine content does not increase any more with the longer chlorination period. Such a developing trend reflects the extent of N-H→N-Cl transformation as a function of chlorination periods. The N-H group can almost transform completely into N-Cl structure after 2 h chlorination treatment. Therefore, the chlorination of poly(ATMP-*co*-MMA) can reach the saturation within 2 h without extending chlorination period.

3.4 Antimicrobial assessment

The as-synthesized products, amine *N*-halamine microspheres, can be utilized as bactericides for treating microorganism as schematically illustrated in scheme 2. For investigation, bacterial suspension was herein selected as simulated water polluted by pathogenic bacteria for testing bactericidal activity of the amine *N*-halamine microspheres. The antibacterial performance of the amine *N*-halamine microspheres was examined against model bacteria *E. coli* and *S. aureus* by using the plate counting method. Fig. 8A shows photographs of the bacterial culture plates, visualizing the survival case of *E. coli* and *S. aureus* after 40 min exposure to the control and amine *N*-halamine microspheres (1.17 % oxidative chlorine content). Survival bacterial colonies on the culture plates are observed as small white dots. Dense bacterial colonies are detected on the control plate for both *E. coli* and *S. aureus*, and it is hardly to discern the aggregated bacteria. Compared with the control plate, obvious decrease is detected in the population of the bacterial colonies after the exposure to the amine *N*-halamine microspheres, reflecting that amine *N*-halamine microspheres have excellent antimicrobial activity towards the model bacteria.

The antibacterial activity of the amine *N*-halamine microspheres was further assessed using the zone of inhibition study as shown in Fig. 8B. Sample was processed into small disc, and the typical Gram-negative bacteria *E. coli* and Gram-positive bacteria *S. aureus* were selected as experimental microorganism. The inhibition zone reflects the susceptibility of the bacteria towards the as-prepared amine *N*-halamine microspheres.[48] For comparison, bacteria without contacting biocides were investigated as control. The cultural plate without sample offers a robust growth of bacteria showing crowded colonies, and has no inhibition zone at all. On contrary, the amine *N*-halamine microspheres provide an apparent inhibition zone with the diameter of 21.4 mm for *E. coli* and 18.1 mm for *S. aureus*. The presence of the inhibition zone around the sample proves that amine *N*-halamine microspheres possess powerful antibacterial activity.

In our previous reports, several kinds of imide and amide type *N*-halamines were designed, and their bactericidal activities were systematically estimated.[24-27] To substantiate the difference among the imide, amide, and amine type *N*-halamine, the biocidal activity of the amine *N*-halamine microspheres was assayed by the minimum inhibitory concentration (MIC) test. MIC means the sample concentration corresponding to the reduction of ≥3 log in the CFU/mL colony numbers. Lower MIC value suggests higher antibacterial activity. As shown in Table S3, the amine *N*-halamine microspheres have the MIC value of 10 mg/mL against both *E. coli* and *S. aureus*, which is much lower than those in our previous reports. Therefore, it is considered that the as-prepared amine *N*-halamine microspheres have higher antibacterial efficacy than the previous *N*-halamines.

3.5 Effect of particle size on antimicrobial activity

Nanosize *N*-halamines can show more advantageous activity than their bulk counterparts due to their smaller size and larger activated surface area.[14,15] As a control, bulk powder *N*-halamine was introduced in this study for antibacterial test to substantiate size effect on biocidal capability. Fig. 9A displays the biocidal histogram to show the survival case of *E. coli* and *S. aureus* after 40 min contacting the control, bulk powder *N*-halamines, and amine *N*-

halamine microspheres. Control experiment shows 100 % survival colonies, whereas bulk powder and amine *N*-halamine microspheres provide decreased colonies, which indicates that both bulk powder and nanosized *N*-halamines possess antimicrobial capability. According to statistics, bulk powder *N*-halamine gives 46.5 % (*E. coli*) and 50.4 % (*S. aureus*) fractional survival, whereas amine *N*-halamine microspheres shows merely 11.8 % and 14.3 %, respectively. Such an enhanced antimicrobial activity of nanosized amine *N*-halamines compared with their bulk counterpart well explicates the size effect presupposition. Therefore, designing *N*-halamines with nanosize is an advisable mean for enhancing antimicrobial capability.

3.6 Effect of contact period on antimicrobial activity

Contact time of *N*-halamines with pathogenic bacteria is one significant factor determining the antimicrobial activity. Antibacterial kinetic test was applied herein to clarify the relationship between contact time and bactericidal behaviour. Fig. 9B displays antibacterial activity of the amine *N*-halamine microspheres towards *E. coli* as a function of contact time within the range from 0 to 320 min. Sample with 1.17 % chlorine loading was chosen for kinetic test. In general, the survival of *E. coli* decreases proportionally with the aging time. Less than five minute exposure to biocides results in about 61 % bacterial mortality, whereas as high as 88 % reduction corresponds with 40 min exposure. Extending contact time over 80 min can lead to complete killing of bacterial colonies. Such a bactericidal trend combining jumping growth with leveling off with the aging time is in good agreement with results in the previous literatures.[23-27] Morphological changes of *E. coli* after treatment were examined by SEM to further analyse the sterilization kinetics of amine *N*-halamine microspheres. Fig. 9D shows the SEM images of *E. coli* before and after treatment with amine *N*-halamine microspheres for different contact period. The intact *E. coli* is both ends obtuse corynebacteria with a smooth surface (yellow arrow, D-1). After 5 min treatment, rod-like shape of *E. coli* with somewhat rugged surface is detected (green arrow, D-2). Roughness of bacterial surface tends to more obvious, and even small holes (blue arrow, D-3) appear after 80 min. Extending contact time to 320 min, bacteria lose the original appearances, and even seriously crevasse (red arrow, D-4) is detected. The results suggest that the amine *N*-halamine microspheres can destroy the bacterial surface structures.

3.7 Effect of oxidative chlorine content on antimicrobial activity

Significance of oxidative chlorine of *N*-halamines for antimicrobial efficiency is irreplaceable. As discussed above, active chlorine content in the amine *N*-halamine microspheres can be facilely controlled by just tuning the chlorination period (Fig. 7). Investigation of the effect of active chlorine content on biocidal efficiency against model microorganism *E. coli* was carried out as well. As shown in Fig. 9C, samples with different chlorine content (0.53%, 0.66 %, 0.81%, 1.17%, 1.18%, 1.22%, and 1.24%) show distinguishable antibacterial efficiency after treating bacteria with amine *N*-halamine microspheres for 40 min. On the general observation, higher chlorine content leads to more powerful antibacterial activity. The sample containing 0.53 % oxidative chlorine can offer 62 % *E. coli* reduction, while 1.17 % chlorine loaded sample can kill as high as 88 % bacteria within 40 min. It is recognized that antibacterial efficiency of *N*-halamines is in proportion to the corresponding chlorine content because higher oxidative chlorine content can provide more activated groups, which can result in improved antibacterial capability.[49] This reasoning is well verified via this chlorine content effect experiment. After thorough inquiry, we also find that antimicrobial efficiency increases dramatically firstly and then tardily to the maximum at point of 1.18 % active chlorine content. Further increase in chlorine loading hinders the bactericidal efficiency, showing slight decrease in bacterial reduction as illustrated in the magnified insert of Fig. 9C. The most possible reason is that although increased chlorine content usually leads to enhanced bactericidal efficacy, it can also render the surface more hydrophobicity, resulting in poorer contact with the bacteria and thus less efficacy. Generally, bacterial reduction trend shows dramatic increase firstly, calm down, and even slight decrease with increasing oxidative chlorine content.

3.8 Stability assay

Amine *N*-halamines are known for long-term stability. To confirm the stability, amine *N*-halamine microspheres were immersed in the deionized water for different soaking periods, and subsequently iodometric/thiosulfate titrated to determine the remaining active chlorine in amine *N*-halamine microspheres. The relationship between oxidative chlorine with immersing times is presented in Fig. 10A and Table S4. It is found that the positive chlorine content decreases slowly within the whole aging range, and the equilibrium of the dissociation of N-Cl bond is achieved at the point of 1.07 % for 48 h, showing only 8.55 % chlorine reduction. It is widely acknowledged that bactericidal behavior of *N*-halamines can be classified mainly into two parts including dissociation of N-Cl bond followed by inactivation (Fig. 10B-1) and direct transfer active chlorine to bacterial receptor (Fig. 10B-2). From the stability assessment, we can conclude that the direct transfer of oxidative chlorine from amine *N*-halamine microspheres to the pathogen bacteria is significantly favoured over hydrolysis. Therefore, amine *N*-halamine microspheres can mainly kill bacteria by contacting. However, from inhibition zone results (Fig. 8B), we can also speculate that at least some of the positive chlorine diffused from the products to kill the bacteria even without contacting. Most possible explanation is that the dissociated chlorine can be consumed by the bacteria, which can disturb the N-Cl dissociation equilibrium. This could promote the dissociation reaction towards the formation of positive chlorine.[50]

4. Conclusions

In summary, we developed an efficient approach for the design and synthesis of amine *N*-halamine microspheres based on 2,2,6,6-tetramethyl-4-piperidinol via the radical copolymerization. The samples were fully characterized by several different techniques like ^{1}N NMR, FTIR, TEM, SEM, XPS and the iodometric/thiosulfate titration. Particle size and structural ATMP content in copolymer can be well controlled by tuning copolymerization periods. The optimum oxidative chlorine content was captured by the chlorination period

effect experiment. Antimicrobial test exhibited that amine *N*-halamine microspheres have excellent bactericidal capability both against Gram-positive and Gram-negative bacteria. Size effect of *N*-halamines on biocidal efficiency was justified by the comparison between bulk powder and nanosize *N*-halamines. The investigations of bactericidal efficiency related to contact period and oxidative chlorine content were performed as well. Stability of amine *N*-halamine microspheres was also studied as a function of the soaking period. We believe that this study opens up the possibility for extensive investigation of the amine *N*-halamines, broading their practical applications in various fields.

Acknowledgements

This research was supported by the National Natural Science Foundation of China (21304044) and the Supported by Program of Higher-level Talents of Inner Mongolia University (30105-125136).

Notes and references

[a]*College of Chemistry and Chemical Engineering, Inner Mongolia University, Hohhot 010021, People's Republic of China. E-mail address: dongali@imu.edu.cn; Tel: +86 471 4992982*
[b]*College of Chemistry, Jilin University, Changchun 130021, People's Republic of China*
[c]*College of Chemistry and Life Science, Changchun University of Technology, Changchun 130012, People's Republic of China*

1 S. Eckhardt, P. S. Brunetto, J. Gagnon, M. Priebe, B. Giese and K. M. Formm, *Chem. Rev.*, 2013, **113**, 4708-4754.
2 R. J. Bull, D. A. Reckhow, X. Li, A. R. Humpage, C. Joll and S. Hrudey, *Toxicology*, 2011, **286**, 1-19.
3 H. B. Kocer, I. Cerkez, S. D. Worley, R. M. Broughton and T. S. Huang, *ACS Appl. Mater. Interfaces*, 2011, **3**, 2845-2850.
4 J. Lee and H. S. Wang, *J. Appl. Polym. Sci.*, 2011, **122**, 2345-2350.
5 K. Barnes, J. Liang, R. Wu, S. D. Worley, J. Lee, R. M. Broughton and T. S. Huang, *Biomaterials*, 2006, **27**, 4825-4830.
6 J. Lin, V. Cammarata and S. D. Worley, *Polymer*, 2001, **42**, 7903-7906.
7 A. E. I. Ahmed, J. N. Hay, M. E. Bushell, J. N. Wardell and G. Cavalli, *J. Appl. Polym. Sci.*, 2010, **116**, 2396-2408.
8 H. B. Kocer, I. Cerkez, S. D. Worley, R. M. Broughton and T. S. Huang, *ACS Appl. Mater. Interfaces*, 2011, **3**, 3189-3194.
9 E. Kenawy, S. D. Worley and R. M. Broughton, *Biomacromolecules*, 2007, **8**, 1359-1384.
10 S. Liu and G. Sun, *Ind. Eng. Chem. Res.*, 2006, **45**, 6477-6482.
11 H. B. Kocer, A. Akdag, S. D. Worley, O. Acevedo, R. M. Broughton and Y. Wu, *ACS Appl. Mater. Interfaces*, 2010, **2**, 2456-2464.
12 Z. Cao and Y. Sun, *ACS Appl. Mater. Interfaces*, 2009, **1**, 494-504.
13 X. Sun, L. Zhang, Z. Cao, Y. Deng, L. Liu, H. Fong and Y. Sun, *ACS Appl. Mater. Interfaces*, 2010, **2**, 952-956.
14 X. Ren, A. Akdag, C. Zhu, L. Kou, S. D. Worley and T. S. Huang, *J. Biomed. Mater. Res. Part A*, 2009, **91**, 385-390.
15 O. Gutman, M. Natan, E. Banin and S. Margel, *Biomaterials*, 2014, **35**, 5079-5087.
16 Q. Dong, Y. Wang, L. Peng, H. Zhang and B. Liu, *Nanotechnology*, 2011, **22**, 215604.
17 J. Song, H. Kim, Y. Jang and J. Jang, *ACS Appl. Mater. Interfaces*, 2013, **5**, 11563-11568.
18 J. Huang, L. Wang, R. Lin, A. Y. Wang, L. Yang, M. Kuang, W. Qian and H. Mao, *ACS Appl. Mater. Interfaces*, 2013, **5**, 4632-4639.
19 Q. Zhu, F. Tao and Q. Pan, *ACS Appl. Mater. Interfaces*, 2010, **2**, 3141-3146.
20 C. Xu, K. M. A. Uddin, X. Shen, H. S. N. Jayawardena, M. Yan and L. Ye, *ACS Appl. Mater. Interfaces*, 2013, **5**, 5208-5213.
21 A. Dong, Q. Zhang, T. Wang, W. Wang, F. Liu and G. Gao, *J. Phys. Chem. C*, 2010, **114**, 17298-17303.
22 A. Dong, J. Huang, S. Lan, T. Wang, L. Xiao, W. Wang, T. Zhao, X. Zheng, F. Liu, G. Gao and Y. Chen, *Nanotechnology*, 2011, **22**, 295602.
23 A. Dong, S. Lan, J. Huang, T. Wang, T. Zhao, W. Wang, L. Xiao, X. Zheng, F. Liu, G. Gao and Y. Chen, *J. Colloid Interface Sci.*, 2011, **364**, 333-340.
24 A. Dong, S. Lan, J. Huang, T. Wang, T. Zhao, L. Xiao, W. Wang, X. Zheng, F. Liu, G. Gao and Y. Chen, *ACS Appl. Mater. Interfaces*, 2011, **3**, 4228-4235.
25 A. Dong, Y. Sun, S. Lan, Q. Wang, Q. Cai, X. Qi, Y. Zhang, G. Gao, F. Liu and C. Harnoode, *ACS Appl. Mater. Interfaces*, 2013, **5**, 8125-8133.
26 A. Dong, Z. Huang, S. Lan, Q. Wang, S. Bao, Siriguleng, Y. Zhang, G. Gao, F. Liu and C. Harnoode, *J. Colloid Interface Sci.*, 2014, **413**, 92-99.
27 A. Dong, M. Xue, S. Lan, Q. Wang, Y. Zhao, Y. Wang, Y. Zhang, G. Gao, F. Liu and C. Harnoode, *Colloid. Surf. B*, 2014, **113**, 450-457.
28 Y. Sun and G. Sun, *J. Appl. Polym. Sci.*, 2001, **80**, 2460-2468.
29 J. Jang and Y. Kim, *Chem. Commun.*, 2008, **34**, 4016-4018.
30 K. Barnes, J. Liang, S. D. Worley, J. Lee, R. M. Broughton and T. S. Huang, *J. Appl. Polym. Sci.*, 2007, **105**, 2306-2313.
31 X. Ren, L. Kou, H. B. Kocer, C. Zhu, S. D. Worley, R. M. Broughton and T. S. Huang, *Colloid. Surf. A*, 2008, **317**, 711-716.
32 Z. Cao and Y. Sun, *J. Biomed. Mater. Res. Part A*, 2008, **85**, 99-107.
33 H. Lu, B. Xu, Y. Dong, F. Chen, Y. Li, Z. Li, J. He, H. Li and W. Tian, *Langmuir*, 2010, **26**, 6838-6844.
34 X. Sun, Z. Cao, N. Porteous and Y. Sun, *Ind. Eng. Chem. Res.*, 2010, **49**, 11206-11213.
35 W. Wang, X. Wang, Q. Yang, X. Fei, M. Sun and Y. Song, *Chem. Commun.*, 2013, **49**, 4833-4835.
(36) W. Wang, Y. Zhang, Q. Yang, M. Sun, X. Fei, Y. Song, Y. Zhang and Y. Li, *Nanoscale*, 2013, **5**, 4958-4965.
37 L. Q. Xu, J. C. Chen, R. Wang, K. Nech, E. Kang and G. D. Fu, *RSC Adv.*, 2013, **3**, 25203-25214.
38 Z. Chen and Y. Sun, *Ind. Eng. Chem. Res.*, 2006, **45**, 2634-2640.
39 Z. Deng, M. Chen and L. Wu, *J. Phys. Chem. C*, 2007, **111**, 11692-11698.
40 T. V. Khai, H. G. Na, D. S. Kwak, Y. J. Kwon, H. Ham, K. B. Shim, H. W. Kim, *J. Mater. Chem.*, 2012, **22**, 17992-18003.
41 Z. Jie, X. Yan, L. Zhao, S. D. Worley and J. Liang, *RSC Adv.*, 2014, **4**, 6048-6054.
42 Z. Jie, X. Yan, L. Zhao, S. D. Worley and J. Liang, *Reac. Funct. Polym.*, 2013, **73**, 1580-1587.
43 J. Luo, N. Porteous and Y. Sun, *ACS Appl. Mater. Interfaces*, 2011, **3**, 2895-2903.
44 F. Hui and C. Debiemme-Chouvy, *Biomacromolecules*, 2013, **14**, 585-601.
45 Y. Sun and G. Sun, *J. Polym. Sci. Part A*, 2001, **39**, 3348-3355.
46 R. V. Padmanabhuni, J. Luo, Z. Cao and Y. Sun, *Ind. Eng. Chem. Res.*, 2012, **51**, 5148-5156.
47 J. Liang, Y. Chen, K. Barnes, R. Wu, S. D. Worley and T. S. Huang, *Biomaterials*, 2006, **27**, 2495-2501.
48 X. Sun, Z. Cao, N. Porteous and Y. Sun, *ACTA Biomater.*, 2012, **8**, 1498-1506.
49 Z. Kang, B. Zhang, Y. Jiao, Y. Xu, Q. He and J. Liang, *Cellulose*, 2013, **20**, 885-893.
50 A. Akdag, S. Okur, M. L. McKee and S. D. Worley, *J. Chem. Theory Comput.*, 2006, **2**, 879-884.

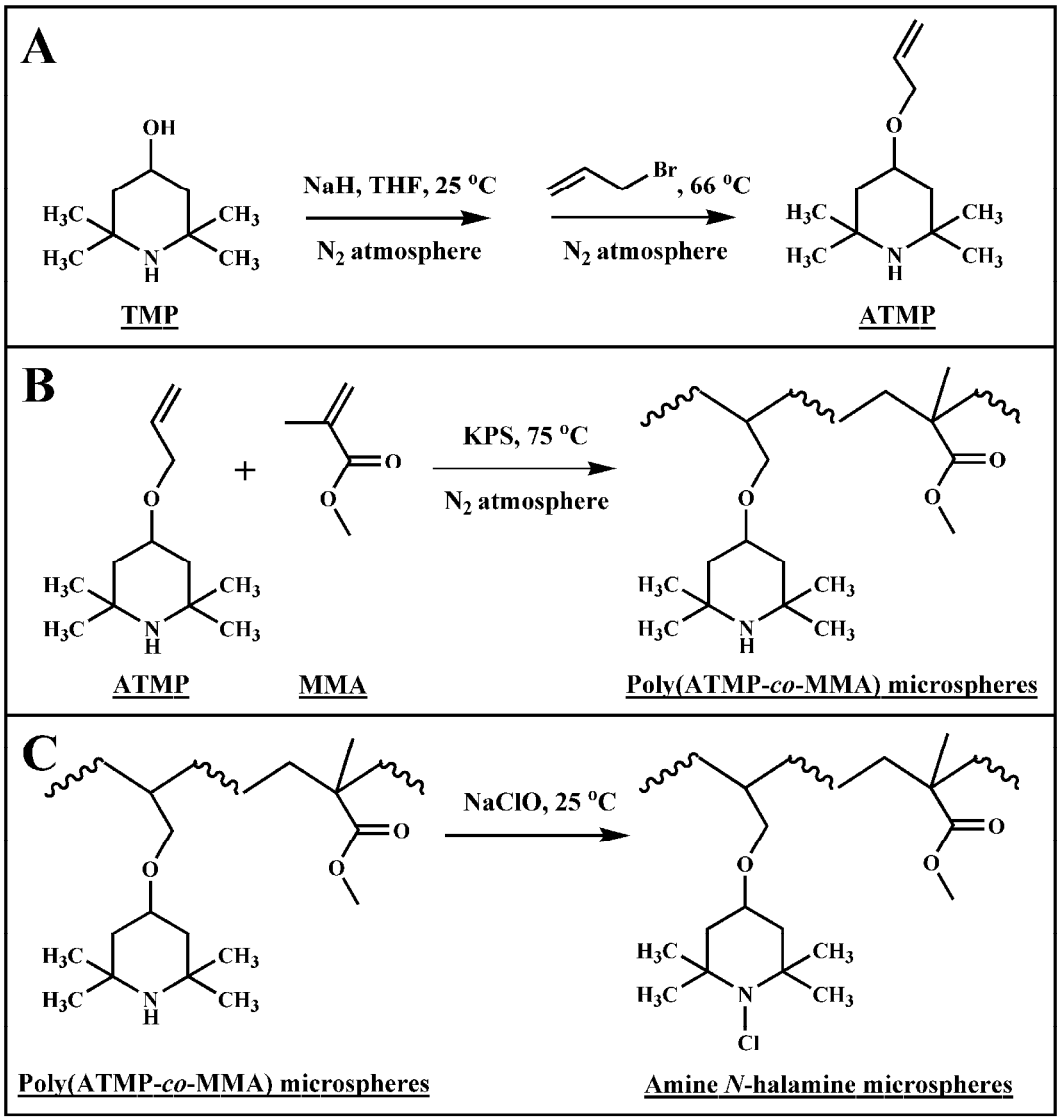

Scheme 1. Schematic illustration of the synthesis of amine *N*-halamine microspheres.

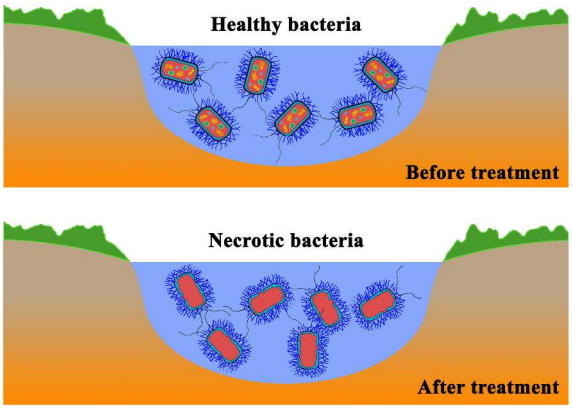

Scheme 2. Picture showing pathogen bacteria treated with amine *N*-halamine microspheres.

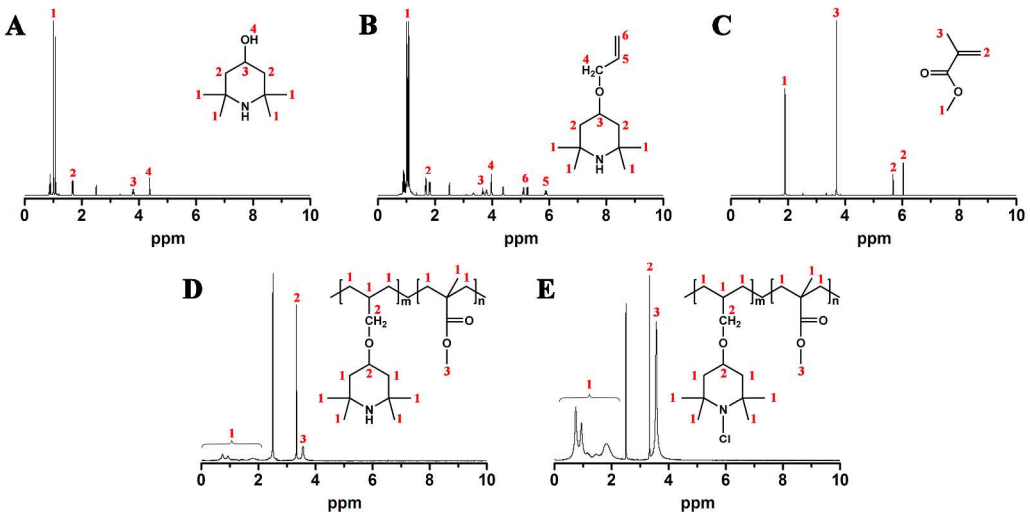

Fig. 1 ^{1}H NMR of TMP (A), ATMP (B), MMA (C), poly(ATMP-*co*-MMA) microspheres (D), and amine *N*-halamine microspheres (E).

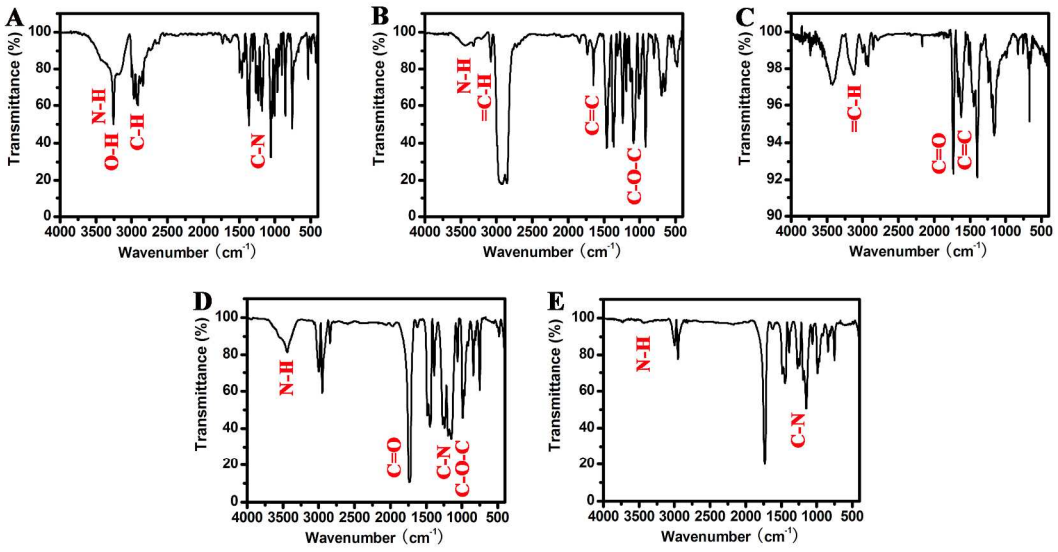

Fig.2. FTIR of TMP (A), ATMP (B), MMA (C), poly(ATMP-*co*-MMA) microspheres (D), and amine *N*-halamine microspheres (E).

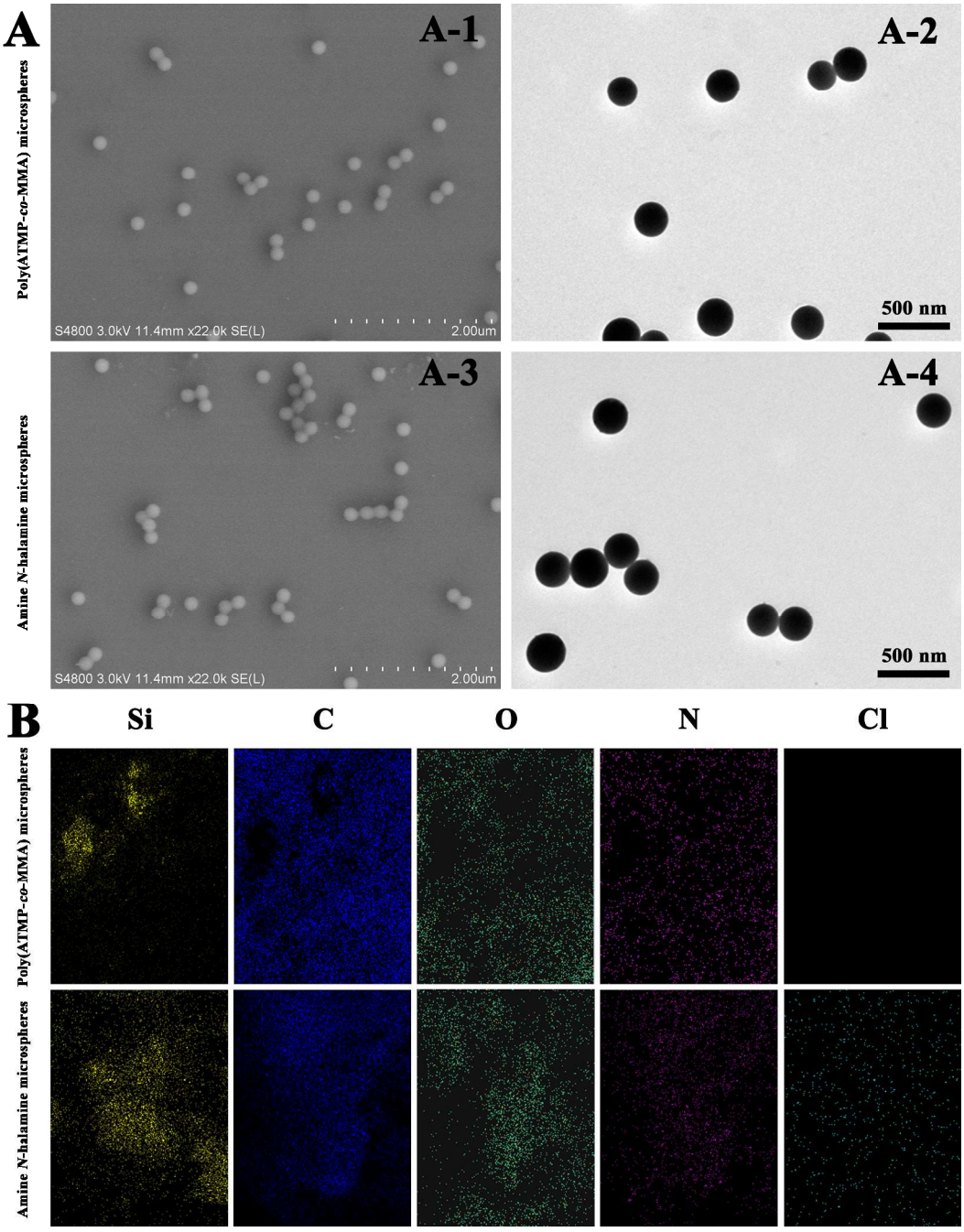

Fig.3. SEM (A-1 and A-3), TEM (A-2 and A-4), and elemental mapping (B) of poly(ATMP-*co*-MMA) microspheres and amine *N*-halamine microspheres.

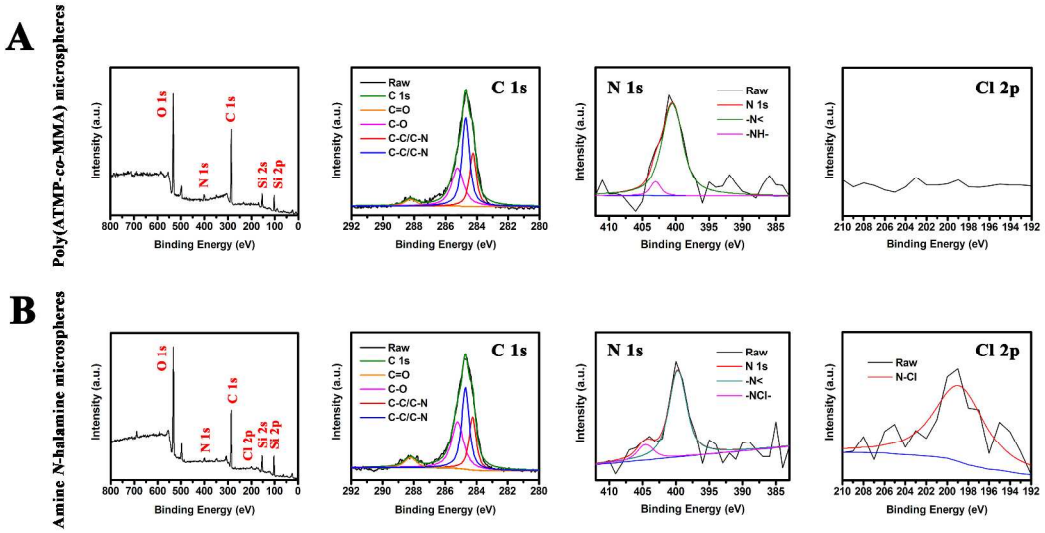

Fig.4. XPS survey scans and high-resolution C 1s, N 1s, and Cl 2p spectra for poly(ATMP-*co*-MMA) microspheres (A) and amine *N*-halamine microspheres (B).

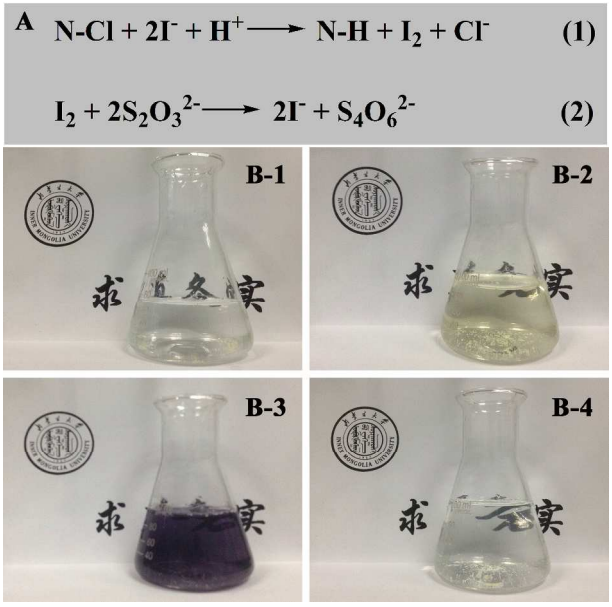

Fig.5. The oxidation-reduction reactions and colour change involved in the iodometric/thiosulfate titration.

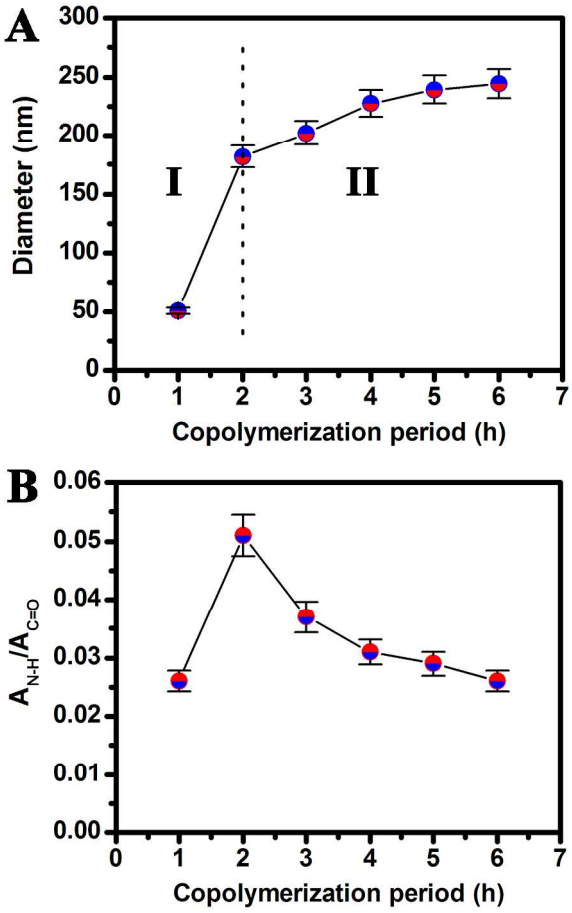

Fig.6. Effect of copolymerization period on particle size (A) and copolymer component (B) of poly(ATMP-*co*-MMA) microspheres.

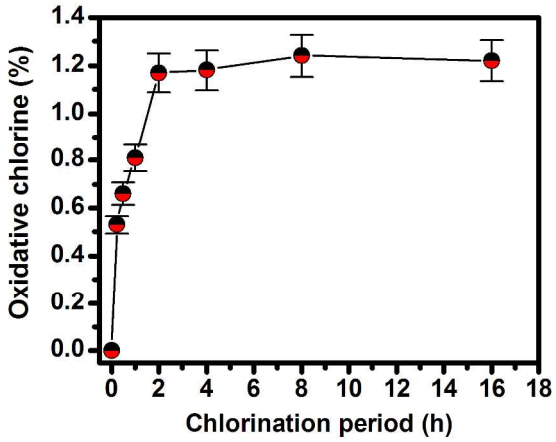

Fig.7. Effect of chlorination period on oxidative chlorine content of amine *N*-halamine microspheres.

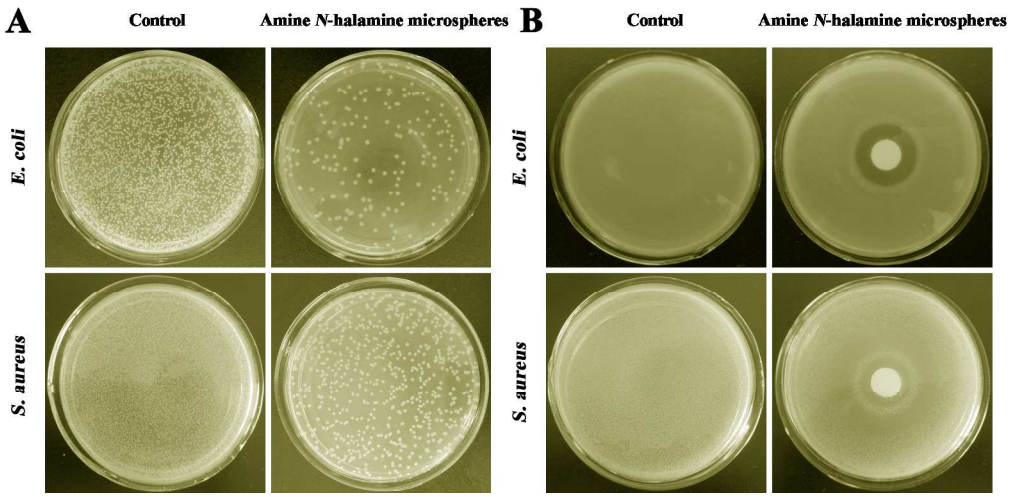

Fig. 8. (A) Photographs showing the bacterial culture plates of *E. coli* and *S. aureus* upon a 40 min exposure of the control and amine *N*-halamine microspheres (1.17 % oxidative chlorine content). (B) Optical images of the zone of inhibition against *E. coli* and *S. aureus* for the control and amine *N*-halamine microspheres (1.17 % oxidative chlorine content).

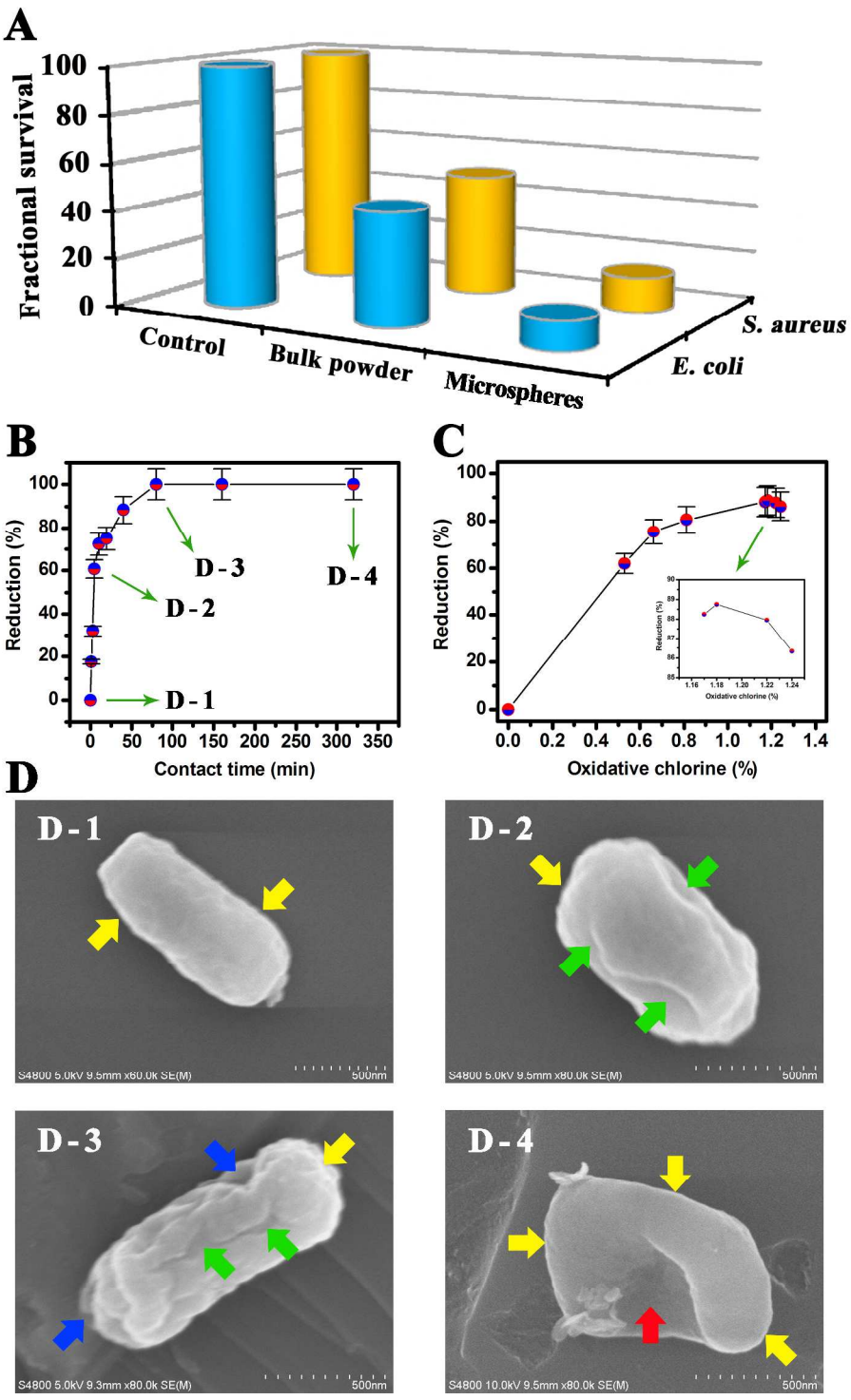

Fig. 9. (A) Survival case of bacterial colonies (*E. coli* and *S. aureus*) upon the exposure to the control, bulk powder *N*-halamine, and amine *N*-halamine microspheres. (B) Antibacterial kinetic test graphs for amine *N*-halamine microspheres against *E. coli*. (C) Effect of oxidative chlorine content of amine *N*-halamine microspheres on antimicrobial activity. (D) SEM images of *E. coli* treated with amine *N*-halamine microspheres for different contacting period.

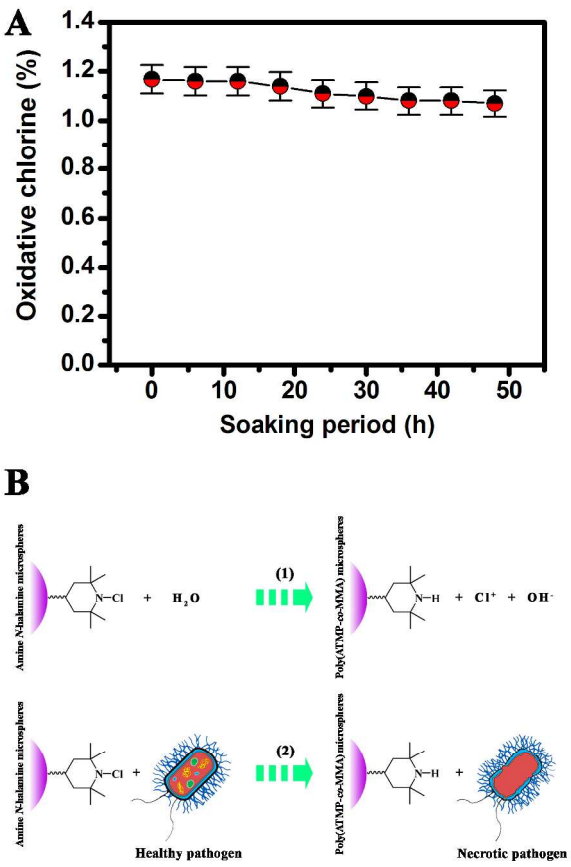

Fig. 10. (A) Oxidative chlorine content of amine *N*-halamine microspheres with different soaking period. (B) Oxidative chlorine transfer scheme from N-Cl bond to water (1) and microorganism (2).